JMEPEG (2020) 29:3784–3791
https://doi.org/10.1007/s11665-020-04896-6

1059-9495/$19.00

In Situ Synthesis of Polycrystalline Cubic Boron Nitride Reinforced by Different Morphologic TiB_2

Shenglin Zhong, Chuan Chen, Zhikai Li, Yang Liu, Bingsai Liu, and Yi Wu1

(Submitted December 2, 2019; in revised form May 13, 2020; published online June 19, 2020)

Polycrystalline cubic boron nitride (PcBN) reinforced by different morphologic titanium diboride (TiB_2) was in situ synthesized in the temperature range of 1100-1600 °C under an ultra-high pressure of 5.5 GPa in cBN-Ti-Al system. The composition and microstructure of PcBN composites were investigated by x-ray diffractometry, scanning electron microscopy and energy-dispersive spectroscopy. The mechanism and influencing factors of TiB_2 microstructure formation with different morphologies were analyzed. The mechanical properties of PcBN were also tested and analyzed. The results showed that the microstructure of TiB_2 evolves from whisker to plate and rod to granular as the temperature increases. Under the combined effects of phase composition, relative density and TiB_2 morphology, the microhardness of PcBN increased continuously, while the flexural strength first increased and then decreased. The high flexural strength was obtained at 1300 and 1400 °C, which were 840.39 and 823.32 MPa, respectively.

Keywords PcBN, TiB_2, in situ synthesis, microstructure, morphology

1. Introduction

Cubic boron nitride (cBN) crystal structure is similar to diamond, which not only has high hardness and high strength, but also has excellent thermal stability and chemical inertness and so on (Ref 1, 2). However, cBN composed of a high-strength covalent bond is difficult to sinter and has anisotropy, which is liable to cause problems such as cleavage during the processing of the material (Ref 3). Polycrystalline cubic boron nitride (PcBN) is a superhard material bonded with cBN by binder. Its unique structure can overcome the defects of cBN cleavage and anisotropy. Therefore, it is widely used in the processing of cast iron and hardened steel and other materials (Ref 4-6).

At present, the commonly used binders for PcBN can be divided into metals, cermets and ceramics. Since PcBN tools have a sharp rise in temperature during cutting, it is more meaningful to use ceramic binders to ensure excellent mechanical properties at high temperatures. However, the brittleness of ceramics leads to a decrease in the toughness of PcBN materials. Therefore, the selection of high-strength, high-hardness, high-toughness ceramic binder combined with cBN to improve the toughness of PcBN is an urgent problem to be solved. Among ceramic binders, titanium diboride (TiB_2) is widely used in tool materials because of its high hardness, high melting point, good chemical stability and excellent thermal conductivity (Ref 7-9). In addition, TiB_2 has a hexagonal C32-type structure, with a lower interfacial energy in the C-axis direction than that in the A-axis direction due to a difference in atomic packing arrangement, so it has a characteristic of preferential growth. Under different Ti-Al-B ratios, TiB_2 ceramics can form equiaxed, plate-like, rod-like structures (Ref 10-13). The plate-like and rod-like structure of ceramics can effectively reduce the stress concentration at the crack tip, leading to crack deflection and bifurcation, as well as the pull-out and bridging of rod crystals, which increases the energy required for crack propagation, thereby greatly increasing the strength and toughness of ceramic materials (Ref 14, 15). Therefore, this paper intends to synthesize different morphologic TiB_2-reinforced PcBN composites by adding Ti and Al alloy micro-powders in cBN under the pressure of 5.5 GPa, sintering temperature of 1100-1600 °C and holding time of 10 min. The microstructure changes of TiB_2 at different temperatures were studied, and their effects on the mechanical properties of PcBN composites were analyzed.

Shenglin Zhong, Chuan Chen, Zhikai Li, Yang Liu, Bingsai Liu, and **Yi Wu**, College of Materials Science and Engineering, Guilin University of Technology, Guilin 541004, China. Contact e-„mail: wuyi1958glut@126.com.

2. Experimental Procedures

2.1 Experimental Materials and Sample Preparation

cBN powders (grain sizes 4-8 μm, purity>99.9 wt.%, Zhongnan Jete Super abrasives Co., Ltd, Zhengzhou, China), Ti powders (grain sizes 3-5 μm, purity>99.6 wt.%, Sinopharm Shanghai Chemical Reagent Co., Ltd, Shanghai, China) and Al powders (grain sizes 2-3 μm, purity>99.8 wt.%, Yuanyang Aluminum Co., Ltd, Henan, China) were used as the raw materials. The mass percentages of the raw materials were 78.68 wt.% cBN, 16.65 wt.% Ti and 4.68 wt.% Al, respectively. The raw materials were ground in an absolute ethanol medium for 2 h by using an agate mortar. Then, the ground powders were dried in an oven for 12 h at 100 °C. After cooling to room temperature, the powders were screened through a 150-mesh sieve. Next, 3.2 g of the ingredients was packed into the cylindrical shell made of molybdenum cup and then vacuum-dried at 120 °C for 12 h. The vacuum-treated samples were chilled into blocks and assembled according to Fig. 1. Finally,

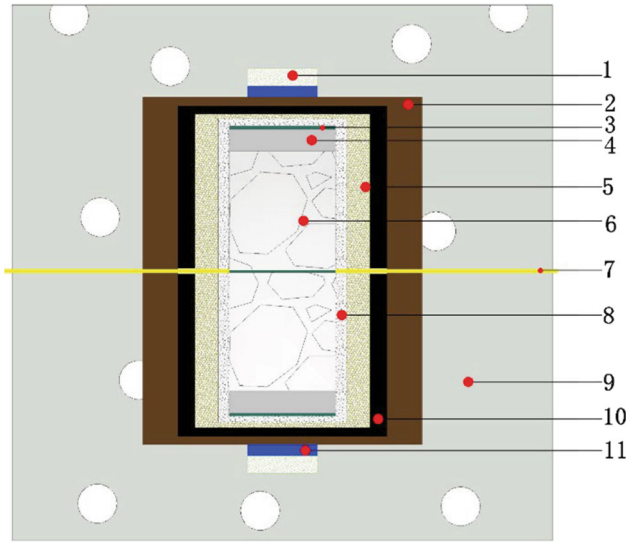

Fig. 1 Sample assembly schematic for the high-temperature and high-pressure sintering experiment: 1—steel ring, 2—zirconia ring, 3—salt sheet (mixed powders of NaCl and C), 4—hard metal, 5—magnesium capsule, 6—samples, 7—thermocouple, 8—pyrophyllite, 9—salt tube, 10—graphite furnace and 11—titanium flake

the samples were synthesized in situ on a hinged six-face hydraulic press. The sintering parameters were set as follows: the sintering pressure (5.5 GPa), the sintering temperature (1100-1600 °C) and the sintering holding time (10 min).

2.2 Sample Characterization

The sintered samples were polished into a mirror surface by a UNIPOL-1502 automatic polishing machine. The relative densities of the samples were calculated as the ratios of experimental densities to theoretical densities. Theoretical densities were calculated according to the mass ratios of the reaction product. The mass of the reaction products was obtained by quantitative analysis of x-ray diffraction. Experimental densities were measured by the Archimedes method. The microhardness of the samples was measured by Vickers microhardness tester (VH-5LDC) with 5000 gf of extrinsic load and a 15 s dwell time, and five positions surfaces were, respectively, tested to determine the microhardness average value. The three-point bending strength of the samples was measured by universal material testing machine (AG-150 KN) with a span of 10 mm and a load speed of 0.5 mm min^{-1}. Phase compositions of the sample were analyzed using x-ray diffraction (XRD) (X'Pert PRO, PANalytical, Netherlands). The microstructures were analyzed using scanning electron microscope (SEM, S-4800, Hitachi High-Technologies Corporation/Oxford Instruments, Japan/England), and the elemental composition was analyzed by energy-dispersive spectrometer (EDS).

3. Results and Discussion

3.1 X-ray Diffraction Analysis

Figure 2 shows the XRD pattern of PcBN at different temperatures. It can be seen from the XRD pattern the phases of

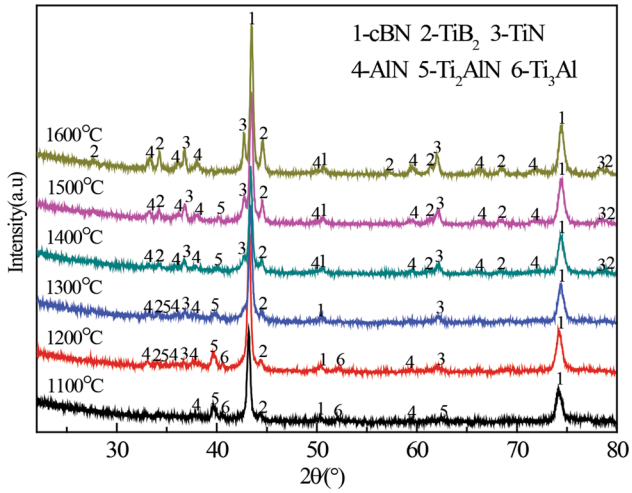

Fig. 2 XRD patterns of PcBN at different sintering temperatures

the sample, including BN, TiB_2, AlN, Ti_2AlN, Ti_3Al at a sintering temperature of 1100 °C. Al has a melting point of 660 °C, which first melts into a liquid phase in the system. Ti, Al and cBN reacted with each other to form Ti_3Al, TiB_2, AlN, Ti_2AlN under the action of liquid phase Al mass transfer (Ref 16-18). The possible chemical reactions are as follows:

$$Al + 3Ti = Ti_3Al \quad \text{(Eq 1)}$$

$$Al + BN = AlN + B* \quad \text{(Eq 2)}$$

$$2BN + 2Al + 2Ti = Ti_2AlN + AlN + 2B* \quad \text{(Eq 3)}$$

$$2Ti + B* = TiB_2. \quad \text{(Eq 4)}$$

As the sintering temperature increased to 1200 °C, the TiN diffraction peak appeared in the XRD pattern, indicating that a new phase of TiN was formed in the sample. When the sintering temperature was 1300 °C, the Ti_3Al diffraction peak disappeared in the spectrum. According to the literature, Ti_3Al may react completely with BN (Ref 19), and the following chemical reactions occur:

$$2Ti_3Al + 4BN = 2TiB_2 + 2TiN + AlN + Ti_2AlN. \quad \text{(Eq 5)}$$

When the sintering temperature was raised from 1400 to 1600 °C, no new phase diffraction peaks were formed, but the diffraction peak intensity of Ti_2AlN was weakened, indicating that the Ti_2AlN in the sample continuously participates in the reaction with increasing temperature, and when the temperature reached 1600 °C, Ti_2AlN reacted completely with BN to form TiB_2, TiN and AlN. It may react as follows:

$$3Ti_2AlN + 4BN = 2TiB_2 + 4TiN + 3AlN. \quad \text{(Eq 6)}$$

Based on XRD and related literature analysis, we have summarized the reaction types and products at different temperatures (Table 1). In this experiment, as the sintering temperature increased (1100-1600 °C), the reaction between cBN, Ti and Al was favored. At 1600 °C, the final compositions included cBN, TiB_2, AlN and TiN. Therefore, the total reaction equation in the cBN-Ti-Al system at a high pressure of 5.5 GPa, a sintering temperature of 1100-1600 °C and a holding time of 10 min as follows:

Table 1 Composition and possible chemical reactions

T, °C	Composition	Chemical reactions
1100	cBN, TiB_2, AlN, Ti_2AlN, Ti_3Al	$Al + 3Ti = Ti_3Al$ (1) $Al + BN = AlN + B*$ (2)
1200	cBN, TiB_2, AlN, Ti_2AlN, Ti_3Al, TiN	$2BN + 2Al + 2Ti = Ti_2AlN + AlN + 2B*$ (3) $2Ti + B* = TiB_2$ (4)
1300	cBN, TiB_2, AlN, Ti_2AlN, TiN	$2Ti_3Al + 4BN = 2TiB_2 + 2TiN + AlN + Ti_2AlN$ (5)
1400	cBN, TiB_2, AlN, Ti_2AlN, TiN	
1500	cBN, TiB_2, AlN, Ti_2AlN, TiN	$3Ti_2AlN + 4BN = 2TiB_2 + 4TiN + 3AlN$ (6)
1600	cBN, TiB_2, AlN, TiN	

Table 2 EDS elemental results of regions in Fig. 3(a)

	A region		B region		C region	
Element	wt.%	at.%	wt.%	at.%	wt.%	at.%
B	47.73	54.39	26.13	46.41	24.25	47.80
N	51.62	45.39	19.38	26.57	11.80	18.82
Al	0.26	0.12	16.69	11.87	5.26	4.96
Ti	0.39	0.10	37.80	15.15	58.69	28.42

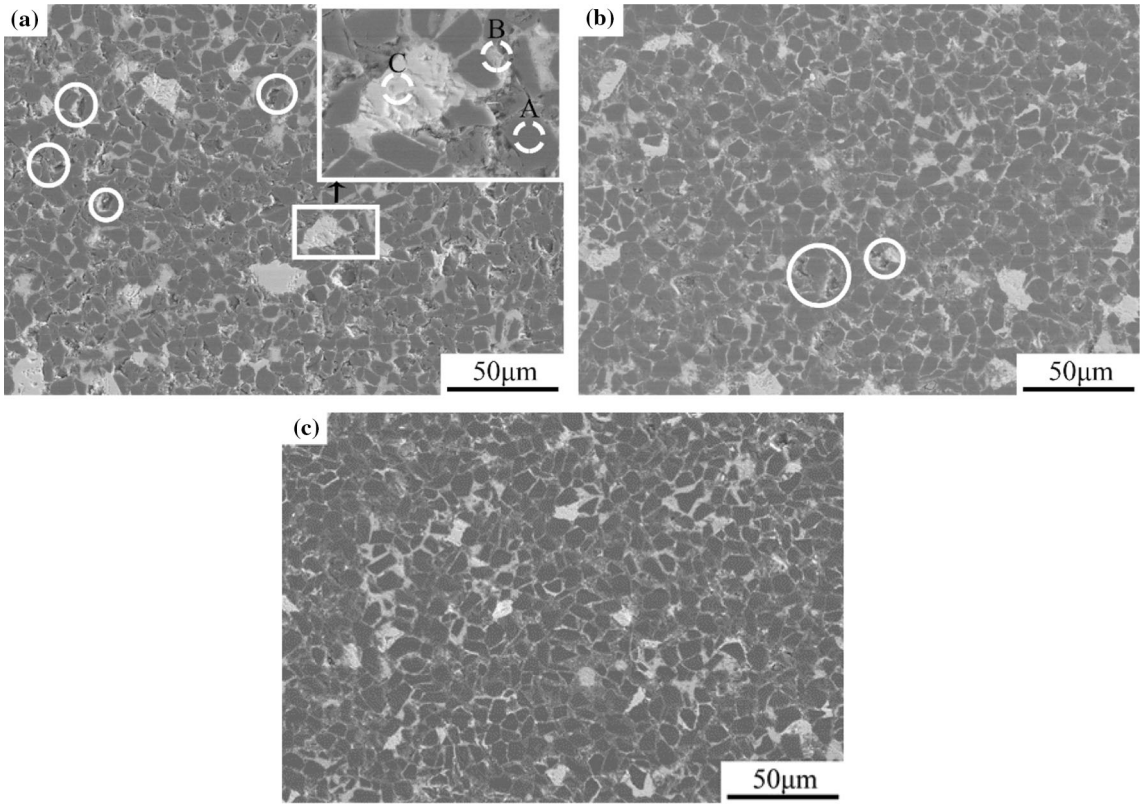

Fig. 3 The backscattered electron images of PcBN polished surface synthesized in situ at different sintering temperatures: (a) 1100 °C; (b) 1300 °C; (c) 1600 °C

$$Al + 2Ti + 2BN = TiB_2 + TiN + AlN. \quad \text{(Eq 7)}$$

3.2 SEM Analysis

Figure 3 presents the backscattered electron images of PcBN polished surface synthesized in situ at different sintering temperatures. The polished surface of the sample is mainly composed of black, gray and white (Fig. 3). Combined with XRD analysis and EDS results (Table 2), the black (A region) region is mainly rich in B and N elements, corresponding to cBN. There is a gray bonding layer (B region) around cBN. EDS results demonstrated that the gray areas were rich in Al, Ti, B and N, which was the mixed phase of other phases. The white area (C region) has the same elemental composition as the gray area, and the main difference is the higher Ti content in white area.

At low temperatures, there were more white agglomeration areas on the polished surface of the sample, and the degree of phase shedding was more serious (black circles). With increasing sintering temperature, the agglomeration of the white surface of the sample surface decreased, the binder phase firmly bonded the cBN particles together, and the shedding material decreased. At low temperatures, the reason for this phenomenon is that the diffusion rate of each atom in the system is low, which is not conducive to the uniform distribution of the phase, resulting in agglomeration of the binder phase and many white agglomeration regions. Moreover, the reaction between the elements in the system is insufficient, and a variety of unstable phases are generated, resulting in low interfacial bonding strength and phase fall off. As the temperature increases, the diffusion rate of each atom in the system increases, and the reaction between the elements is sufficient to obtain a stable phase. Therefore, the degree of agglomeration and shedding of the phase in the sample was reduced, and the bonding strength between the cBN–cBN particles was improved.

Figure 4 displays the SEM images of the fresh cross sections of PcBN samples with different sintering temperatures after the flexural strength test. When the sintering temperature is 1100 °C, there are more pores in the cross section of the sample, the binding force between the cBN and the bonding agent is weak, and the overall structure is relatively loose. As the temperature increases, the cross-sectional structure of the sample becomes tight, the internal pores are significantly reduced, and the density is significantly increased. The main reason is that the liquid phase of the system increases and the viscosity decreases with the increases in sintering temperature, which accelerating the flow of atoms and aggravating the occurrence of chemical reactions. At the same time, the shrinkage of the sintered body increases and the pores are further discharged to make the PcBN structure more compact.

Figure 5 displays the cross-sectional SEM image of PcBN samples corroded by high concentration hydrofluoric acid (HF) for 40 s. The main function of HF is to corrode the metal, intermetallic compound and glass phase formed in PcBN, which is beneficial to observe the microstructure of the stable phase cBN, TiB_2, AlN and TiN.

The corrosion morphology of the sample after 1100 °C sintering is mainly composed of two parts: black bulk particles cBN and whisker structure (Fig. 5a). XRD analysis showed that the main phases included BN, TiB_2, AlN, Ti_2AlN and Ti_3Al at 1100 °C. Among these phases, only TiB_2 has preferential growth characteristics due to its hexagonal structure. Combined with EDS results (Table 3), the whisker structure was mainly rich in Ti, B and N. According to the atomic percentage, the whisker structure can be determined as TiB_2. The cBN particles in the sample were connected to each other by whisker-like TiB_2. As the temperature increases, the whisker-like TiB_2 transforms into plate-like shape and thin rod shape (Fig. 5b). When samples were sintered 1400 °C, the rod-shaped and plate-like TiB_2 with different sizes and a sheet-like structure which were agglomerated together appeared in the corrosion appearance diagram (Fig. 5c). EDS analysis showed that the sheet structure was TiN (Table 3). When the temperature reached 1500 °C, the long rod-like and plate-like TiB_2 disappeared in the corrosion profile, and only a small amount

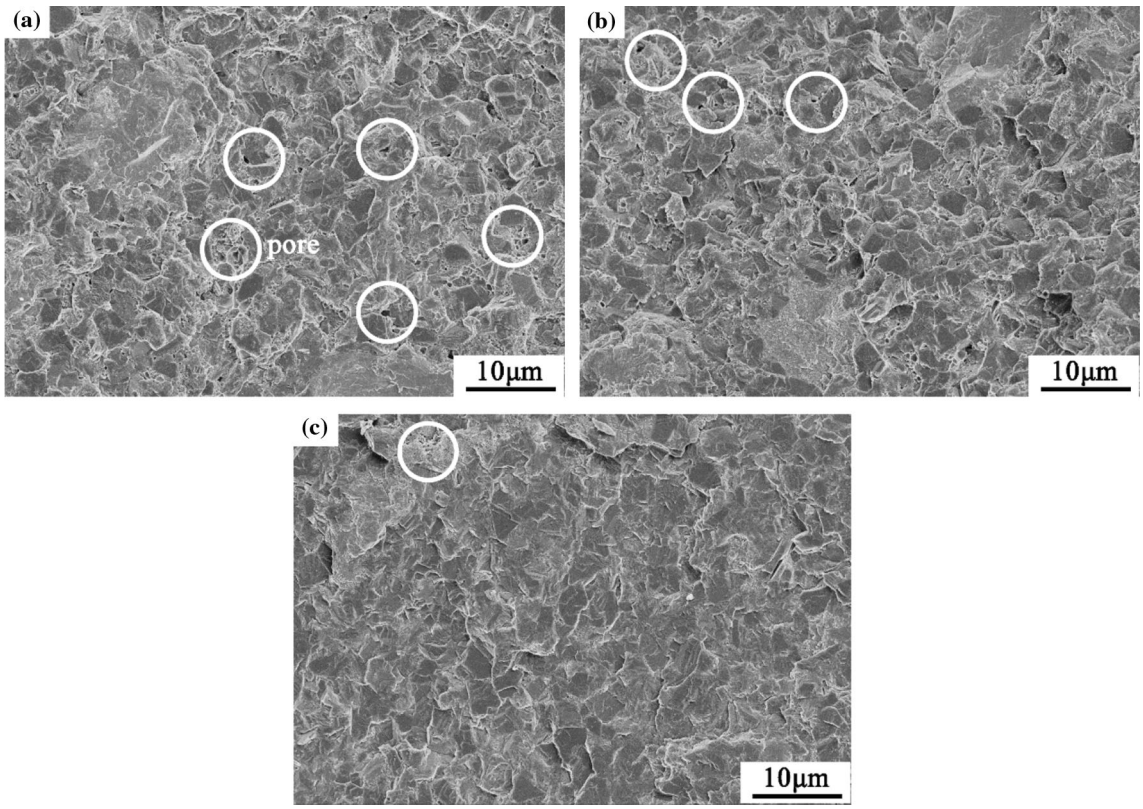

Fig. 4 Fresh cross section SEM images of PcBN samples with different sintering temperatures: (a) 1100 °C; (b) 1300 °C; (c) 1600 °C

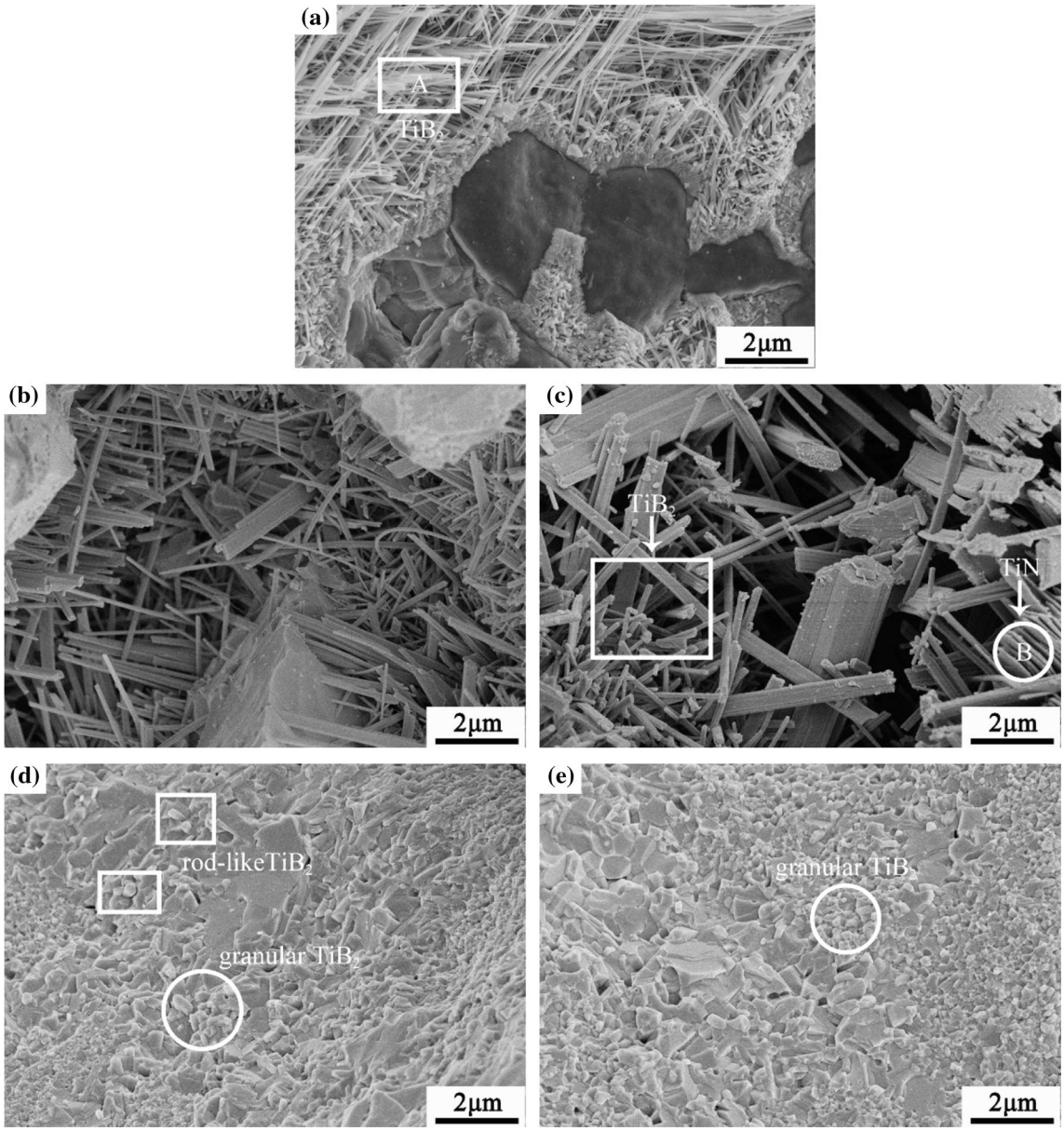

Fig. 5 Corrosion profile of PcBN samples synthesized at different sintering temperatures: (a) 1100 °C; (b) 1300 °C; (c) 1400 °C; (e) 1500 °C; (f) 1600 °C

Table 3 EDS elemental results of regions in Fig. 5(a) and (c)

	A region		B region	
Element	**wt.%**	**at.%**	**wt.%**	**at.%**
B	30.25	59.28	3.18	11.04
N	8.80	10.82	12.88	34.52
Al	2.26	1.98	0.92	1.29
Ti	58.69	27.92	83.02	53.15

of short rod-like TiB_2 (Fig. 5d rectangular frame) and a large amount of fine granular TiB_2 (Fig. 5d circular frame) were observed. When the temperature had risen to 1600 °C, the morphology of TiB_2 was granular (Fig. 5e). According to the Ti-Al-B ternary alloy phase diagram and the previous studies (Ref 20-22), the Ti-Al liquid phase and B content ratio affected the formation of TiB_2 morphology. In the Ti-Al-B system, when the content of B is small, the morphology of TiB_2 is mainly whisker like. With the increases in B content, whisker-like TiB_2 gradually changes to plate and rod crystal. As the content of B continues to increase, rod-like TiB_2 transition to granular. In the cBN-Ti-Al system, Al reacted with BN to form

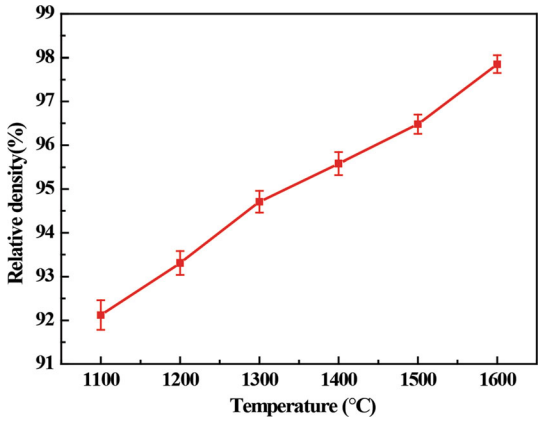

Fig. 6 Relative density of the PcBN at different sintering temperatures

AlN and displaced B atoms. The variation of sintering temperature changed the proportion of Ti-Al liquid phase and B content in the system. At low temperature (1100-1200 °C), the reaction between Al and cBN was insufficient, and the B atoms obtained by the substitution were less, resulting in the morphology of TiB_2 being mainly whisker. The rise of temperature is conductive to the reaction between Al and cBN, and the content of B atom obtained by substitution increases. Hence, the whisker-like TiB_2 was transformed into a plate-like or rod-like shape. When the temperature reached 1600 °C, Al reacted completely with cBN to form AlN, and the excess B atoms were replaced, resulting in the conversion of plate-like or rod-like TiB_2 into fine particles.

3.3 Relative Density

The relative density of PcBN composites increased with increasing sintering temperature (Fig. 6), indicating that the increase in sintering temperature promoted the densification of PcBN samples. On the one hand, Al metal with low melting point is added to the binder. When the temperature reaches the melting point of Al, it melts to form a liquid phase. The sintering mode of the system changes from a solid phase to a liquid phase. When the temperature rises, the viscosity of the liquid phase in the system decreases, and the diffusion rate of Al and Ti atoms is accelerated, which not only fills the gap in the sintered body and avoids the generation of pores, but also promotes the chemical reaction between the binder and cBN and the uniformity of the phase distribution. Moreover, as the temperature rises accelerates the discharge of PcBN internal gas and the flow and rearrangement between the powder particles under ultra-high pressure conditions. The sample shrinkage rate increased and the densification rate increased. On the other hand, there are many phases formed in the sample at low temperatures, and the coefficients of thermal expansion between the phases are different. Therefore, it was easy to cause thermal stress concentration in the sample, resulting in micropores or microcracks, which caused the sample density to decrease.

3.4 Vickers Hardness and Flexural Strength

The microhardness of PcBN increases with the increase in temperature, which is consistent with the change of relative density (Fig. 7a). First, the greater the relative density, the

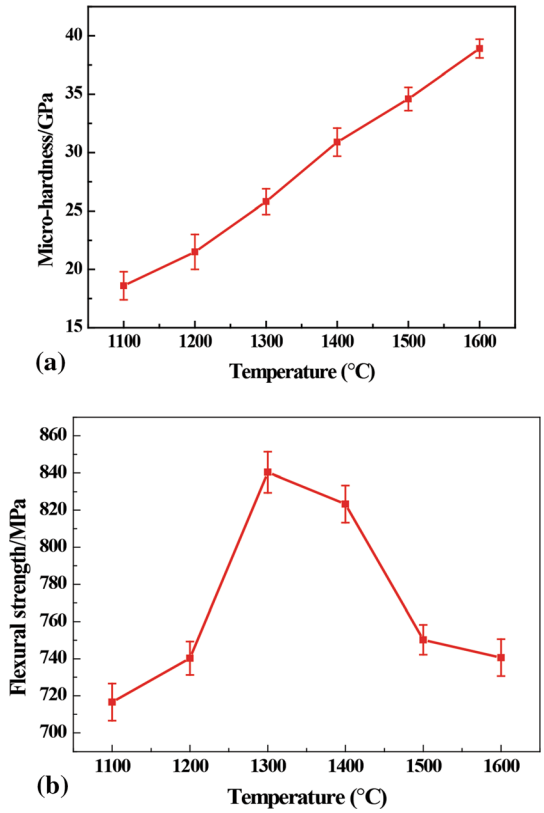

Fig. 7 The mechanical properties of the PcBN at different sintering temperatures: (a) microhardness; (b) flexural strength

higher the microhardness (Ref 23). The relative density of PcBN increased gradually with increasing the sintering temperature from 1100 to 1600 °C, resulting in the increase in microhardness. Second, the high temperature is favorable for the progress of the reaction, making ability of the binder to bond with the cBN is enhanced, promoting an increase in the hardness of the sample. Third, at low temperatures, Ti_3Al and Ti_2AlN with low microhardness are present in the sample (Ref 24, 25), resulting in low hardness of the PcBN composite. The Ti_3Al and Ti_2AlN phases in the PcBN composites decrease slowly with the increase in temperature. At 1600 °C, only cBN, AlN, TiN and TiB_2 stable ceramic phases existed in the sample. At this time, the hardness of the sample reached a maximum of 38.9 GPa.

The change in the flexural strength of PcBN was inconsistent with the microhardness. The flexural strength increases first and then decreases with increasing sintering temperature (Fig. 7b). The reason for this change is due to the density of the sintered sample and the change of the TiB_2 morphology of the reinforcing phase in PcBN. On the one hand, the flexural strength of a material generally decreases as the relative density decreases. The low relative density of the material indicates that the material has high porosity. Porosity, as a defect, often becomes a source of cracking. The pores reduce the effective cross-sectional area of the applied load, resulting in a reduction in the force that the material can withstand. Moreover, the pores easily lead to stress concentration and microcracks in the adjacent area, causing the material to break under low force (Ref 26). When the sintering temperature increased from 1100 to 1300 °C, the flexural strength of the PcBN increased with the

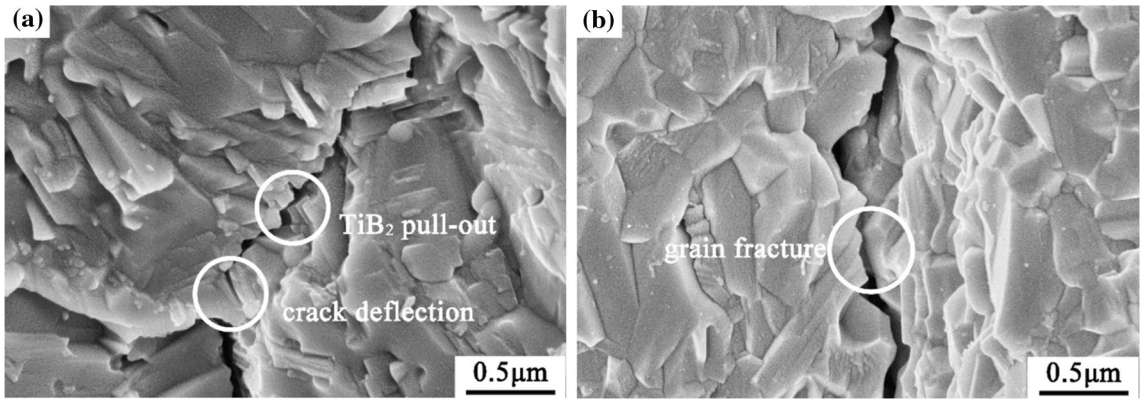

Fig. 8 SEM images of crack deflection and rod crystal pull-out and fracture of the sintered sample at 1300 °C

Table 4 Comparison of the mechanical properties of similar composite materials with the results of this work

Reference	Composite material	Sintering conditions	Microhardness, GPa	Flexural strength, MPa
17	cBN-AlN	1600 °C/5GPa	29	…
27	cBN-TiN-Al	1400 °C/5.8 GPa	30.7	…
28	cBN–Ti_3Al-Al	1600 °C/5GPa	35.04±0.51	…
28	cBN–Ti_3Al	1600 °C/5GPa	~21	…
29	cBN-Ti-Al	1400 °C/50 MPa	14.1±0.5	~390.7±4.4
30	cBN-Al	1350 °C/5.5 GPa	~3000	~250
30	cBN-TiN	1350 °C/5.5 GPa	~2700	~400
31	cBN(SiO_2)-Al-B-C	1700 °C/100 MPa	38±3.5	425±23
32	cBN-Ti-Al-W	1350 °C/5.5 GPa	28.35	673.54
This work	cBN-Ti-Al	1300 °C/5.5 GPa	25.8	840.39
	cBN-Ti-Al	1400 °C/5.5 GPa	30.9	823.32

relative density, and the flexural strength reached a maximum of 840.39 MPa at 1300 °C.

On the other hand, the morphology of the reinforcing phase TiB_2 has a great influence on the bending strength of the PcBN composite. It is a consensus that ceramic whiskers, plate-like and rod-like structures can enhance toughened ceramic materials (Ref 14, 15). When the material breaks, whisker, plate-like and rod-like structure of ceramics can effectively reduce the stress concentration at the crack tip, leading to crack deflection and bifurcation, as well as the pull-out and fracture of rod crystals, which increases the energy required for crack propagation, thereby greatly increasing the strength and toughness of ceramic materials. As shown in Fig. 8, we can clearly see the rod crystal pull-out, fracture and crack deflection in the microcracks in the cross section of the sintered sample at 1300 °C. Due to the high elastic modulus and strength of the TiB_2 rod crystal, on the one hand, the rod crystal is pulled from the matrix or the crack is deflected around the rod crystal, and the crack propagation path is increased, which will greatly consume the energy of crack propagation. On the other hand, the energy required for the fracture of TiB_2 rods is much higher than that of cBN, so the flexural strength of PcBN is greatly improved. As the temperature continues to rise, the crystal form of the reinforcing phase TiB_2 changed due to the change of the B content, so that the whisker, plate and rod crystal structure of the TiB_2 in the PcBN composite material was continuously reduced. Therefore, when the temperature rose from 1300 to 1600 °C, although the relative density was continuously increased, whiskers, plate-like and rod-like TiB_2 gradually change to the particle structure, and its strengthening effect weakens and the flexural strength decreases continuously.

Table 4 lists the comparison of the mechanical properties of similar composite materials with the results of this work. These data show that good mechanical properties were obtained in the process of in situ synthesis of TiB_2 with different morphologies in the cBN-Ti-Al system to enhance PcBN, especially its bending strength has been greatly improved. Hence, the work in this paper has a good reference for improving the strength of PcBN.

4. Conclusion

In summary, The PcBN reinforced by different morphologic TiB_2 was prepared in the cBN-Al-Ti system under high temperature (1100-1600 °C) and ultra-high pressure (5.5 GPa) with 10 min holding. The phase composition, the chemical reaction mechanism, TiB_2 morphology change process, mechanical properties and strengthening mechanism were studied and analyzed in detail. As the sintering temperature increased, the transition phase of PcBN changed to a stable phase, the uniformity of the distribution was improved, the relative density and microhardness were continuously increased. At the same time, the morphology of the reinforcing phase TiB_2 was constantly changing, from the whisker shape (1100-1200 °C) to the plate shape and rod shape (1300-1400 °C) to the granular shape (1500-1600 °C). Under the influence of phase composition, relative density of the sample and the enhancement of plate and rod-like TiB_2, the flexural strength of the sample first increased and then decreased, and the high bending strengths were obtained at 1300 and 1400 °C, which

were 840.39 and 823.32 MPa, respectively. In addition, how to obtain plate or rod crystal TiB_2-reinforced PcBN at high temperature (1500-1600 °C) should be studied in the future work, which is helpful for preparing high-strength and high-hardness PcBN.

Acknowledgments

This study was financially supported by the Innovation-driven Development Special Fund Project of Guangxi Province, China (AA17204098) and project supported by The Open Research Project of Key Laboratory of Superhard Materials of Guangxi Province, China (2017-K-01).

References

1. G.Z. Wang, 立方氮化硼 (cBN) 特性综述 (Summarization About the Peculiarities of cBN), *Superhard Mater. Eng.*, 2005, **17**(5), p 41–45 ((in Chinese))
2. S. Ono, K. Mibe, N. Hirao, and Y. Ohishi, In Situ Raman Spectroscopy of Cubic Boron Nitride to 90 GPa and 800 K, *J. Phys. Chem. Solids*, 2005, **76**, p 120–124 ((in English))
3. S. Yin, H.Y. Lai, and X.C. Cheng, 立方氮化硼烧结体的显微结构和烧结机理 (Microstructure and Sintering Mechanism of Sintered Cubic Boron Nitride Materials), *J. Chin. Ceram. Soc.*, 1984, **12**(4), p 450–455 ((in Chinese))
4. L. Chen, J.E. Stahl, W. Zhao, and J.M. Zhou, Assessment on Abrasiveness of High Chromium Cast Iron Material on the Wear Performance of PCBN Cutting Tools in Dry Machining, *J. Mater. Process. Technol.*, 2018, **255**, p 110–120 ((in English))
5. X.L. Liu, S.Y. Li, T. Chen, and D.Y. Wang, Research on the Surface Characteristics of Hardened Steel with Variable Chamfer Edge PCBN Insert by High-Speed Hard Turning, *Int. J. Precis. Eng. Manuf.*, 2018, **19**(2), p 157–165 ((in English))
6. M. Ociepa, M. Jenek, and E. Feldshtein, On the Wear Comparative Analysis of Cutting Tools Made of Composite Materials Based on Polycrystalline Cubic Boron Nitride When Finish Turning of AISI, D2 (EN X153CrMoV12) Steel, *J. Superhard Mater.*, 2018, **40**(6), p 396–401 ((in English))
7. D.S. King, W.G. Fahrenholtz, and G.E. Hilmas, Silicon Carbide-Titanium Diboride Ceramic Composites, *J. Eur. Ceram. Soc.*, 2013, **33** (15–16), p 2943–2951 ((in English))
8. Q. Wen, Y.Q. Tan, Z.H. Zhong, H.B. Zhang, and X.S. Zhou, High Toughness and Electrical Discharge Machinable B_4C-TiB_2-SiC Composites Fabricated at Low Sintering Temperature, *Mater. Sci. Eng. A*, 2017, **701**, p 338–343 ((in English))
9. S.G. Huang, K. Vanmeensel, O. Van der Biest, and J. Vleugels, In Situ Synthesis and Densification of Submicrometer-Grained B_4C-TiB_2 Composites by Pulsed Electric Current Sintering, *J. Eur. Ceram. Soc.*, 2011, **31**(4), p 637–644 ((in English))
10. A.A. Abdel-Hamid, S. Hamar-Thibault, and R. Hamar, Crystal Morphology of the Compound TiB_2, *J. Cryst. Growth*, 1985, **71**(3), p 744–750 ((in English))
11. J.S. Li, F. Zhao, S. Li, M.Y. Wang, and X.J. Wu, 燃烧剂对二硼化钛晶体形态的影响 (Effect of Combustion Agent on the Crystal Morphology of TiB_2), *Rare Met. Mater. Eng.*, 2015, **44**(S1), p 332–335 ((in Chinese))
12. H. Zhang, W.L. Gao, Y.X. Jin, and S.Y. Zeng, Evolution of Solid–Liquid Interface Morphology of Primary TiB_2 in Non-equilibrium Solidified Ti-Al-B Alloys, *Trans. Nonferrous Met. Soc. China*, 2002, **12**(3), p 437–440 ((in English))
13. W.L. Gao, H. Zhang, E.L. Zang, and S.Y. Zeng, TiAl-B合金中初生TiB_2晶体的表面形貌和形成机制 (Surface Morphology and Growth Mechanism of Primary TiB_2 in TiAl-B Alloys), *Mater. Sci. Technol.*, 2002, **10**(4), p 387–390 ((in Chinese))
14. L. Xu, C.Z. Huang, H.L. Liu, B. Zou, H.T. Zhu, G.L. Zhao, and J. Wang, In Situ Synthesis of ZrB_2–ZrC_X Ceramic Tool Materials Toughened by Elongated ZrB_2 Grains, *Mater. Des.*, 2013, **49**, p 226–233 ((in English))
15. G.L. Zhao, C.Z. Huang, H.L. Liu, B. Zou, H.T. Zhu, and J. Wang, Microstructure and Mechanical Properties of TiB_2–SiC Ceramic Composites by Reactive Hot Pressing, *Int. J. Refract. Met. Hard Mater.*, 2014, **42**, p 36–41 ((in English))
16. J. Qian, D. Mukhopadhyay, K.D. Nguyen, K.B. Bertagnolli, and Y. Ma, Sintering of Polycrystalline Boron Nitride Composites for In Situ Synchrotron High Pressure Research, *Int. J. Refract. Met. Hard Mater.*, 2015, **49**, p 288–291 ((in English))
17. R. Lv, J. Liu, Y.J. Li, S.C. Li, Z.L. Kou, and D.W. He, High Pressure Sintering of Cubic Boron Nitride Compacts with Al and AlN, *Diamond Relat. Mater.*, 2008, **17**(12), p 2062–2066 ((in English))
18. E. Benko, P. Klimczyk, J. Morgiel, A. Włochowicz, and T.L. Barr, Electron Microscopy Investigations of the cBN-Ti Compound Composites, *Mater. Chem. Phys.*, 2003, **81**(2–3), p 336–340 ((in English))
19. W.L. Yu, J.L. Wang, Y. Wu, Z.G. Zou, Q.F. Yu, and P.C. Mo, In Situ Synthesis of Polycrystalline Cubic Boron Nitride with High Mechanical Properties Using Rod-Shaped TiB_2 Crystals as the Binder, *Adv. Appl. Ceram.*, 2017, **116**(8), p 419–427 ((in English))
20. M.E. Hyman, C. Mccullough, C.G. Levi, and R. Mehrabian, Evolution of Boride Morphologies in TiAl-B Alloys, *Metall. Trans. A*, 1991, **22** (7), p 1647–1662 ((in English))
21. H. Zhang, W.L. Gao, E.L. Zhang, and S.Y. Zeng, TiAl-B 合金片状TiB_2 晶体表面结构及其生长机理 (Surface Structure and Growth Mechanism of TiB_2 Plate in TiAl-B Alloys), *Acta Mater. Compos Sin.*, 2002, **19**(2), p 45–48 ((in Chinese))
22. W.L. Gao, H. Zhang, E.L. Zhang, and S.Y. Zeng, TiAl-B 合金中TiB_2 微观形态的主要存在方式 (Existing Way of the Morphology of TiB_2 in TiAl-B Alloy), *Foundry Technol.*, 2003, **24**(3), p 176–178 ((in Chinese))
23. Y.J. Liu, D.W. He, P. Wang, X.Z. Yan, C. Xu, F.M. Liu, J. Liu, and Q. W. Hu, Microstructural and Mechanical Properties of cBN-Si Composites Prepared from the High Pressure Infiltration Method, *Int. J. Refract. Met. Hard Mater.*, 2003, **61**, p 1–5 ((in English))
24. Y.L. Chen, Z.Y. Li, J. Tang, C.W. Zeng, W. Gao, X. Yan, and M. Yan, Microstructure, Densification, Microhardness and Antioxidant Properties of Ti_2AlN/TiN FGM Fabricated by Hot-Pressing, *J. Wuhan Univ. Technol. Mater. Sci. Ed.*, 2014, **29**(6), p 1173–1177 ((in English))
25. B.Q. Chen, H.P. Xiong, S.Q. Guo, B.B. Sun, B. Chen, and S.Y. Tang, Microstructure and Mechanical Properties of Dissimilar Welded Ti_3Al/Ni-Based Superalloy Joint Using a Ni-Cu Filler Alloy, *Metall. Mater. Trans. A*, 2015, **46**(2), p 756–761 ((in English))
26. C.P. Zhang, X.W. Gao, H.Q. Ru, W.K. Sun, J.H. Zhu, and H. Zong, 成形压力对SiC/TiB_2 复合材料组织与性能的影响 (Effect of Forming Pressure on Microstructure and Mechanical Properties of SiC/TiB_2 Composites), *J. Inorg. Mater.*, 2017, **32**(5), p 502–508 ((in Chinese))
27. X.Z. Rong, T. Tsurumi, O. Fukunaga, and T. Yano, High-Pressure Sintering of cBN-TiN-Al Composite for Cutting Tool Application, *Diamond Relat. Mater.*, 2002, **11**(2), p 280–286 ((in English))
28. Y. Li, Z.L. Kou, H.K. Wang, K.X. Wang, H.C. Tang, Y.F. Wang, S.Z. Liu, X.T. Ren, C.M. Meng, and Z.G. Wang, High Pressure Sintering Behavior and Mechanical Properties of cBN–Ti_3Al and cBN–Ti_3Al-Al Composite Materials, *High Pressure Res.*, 2012, **32**(4), p 524–531 ((in English))
29. Y.G. Yuan, X.Z. Cheng, R. Chang, T.H. Li, J.B. Zang, Y.H. Wang, Y.Q. Yu, J. Lu, and X.P. Xu, Reactive Sintering cBN-Ti-Al Composites by Spark Plasma Sintering, *Diamond Relat. Mater.*, 2016, **69**, p 138–143 ((in English))
30. L.Y. Yang, Z.M. Yue, J.H. Gong, X.D. Zhao, and X.H. Chu, Compositions, Mechanical Properties and Microstructures of cBN-Based Composites Sintered with Al or TiC, *Adv. Appl. Ceram.*, 2017, **116**(5), p 254–259 ((in English))
31. J. Li, Y. Ma, L.X. Liang, H.L. Wang, and R. Zhang, 放电等离子烧结聚晶立方氮化硼刀具的性能 (Properties of Polycrystalline Cubic Boron Nitride Prepared by Spark Plasma Sintering), *Mater. Mech. Eng.*, 2019, **43**(1), p 8–12 ((in Chinese))
32. P.M. Mo, C. Chen, J.R. Chen, G. Jia, D.L. Xie, L.Y. Xiao, X.Y. Pan, and F. Ling, Effect of Sintering Temperature on Synthesis of PCBN in cBN-Ti-Al-W System, *Diamond Relat. Mater.*, 2020, https://doi.org/10.1016/j.diamond.2020.107714